iScience

CellPress
OPEN ACCESS

Article

Tree root-inspired robust superhydrophobic coatings with high permeation for porous structures

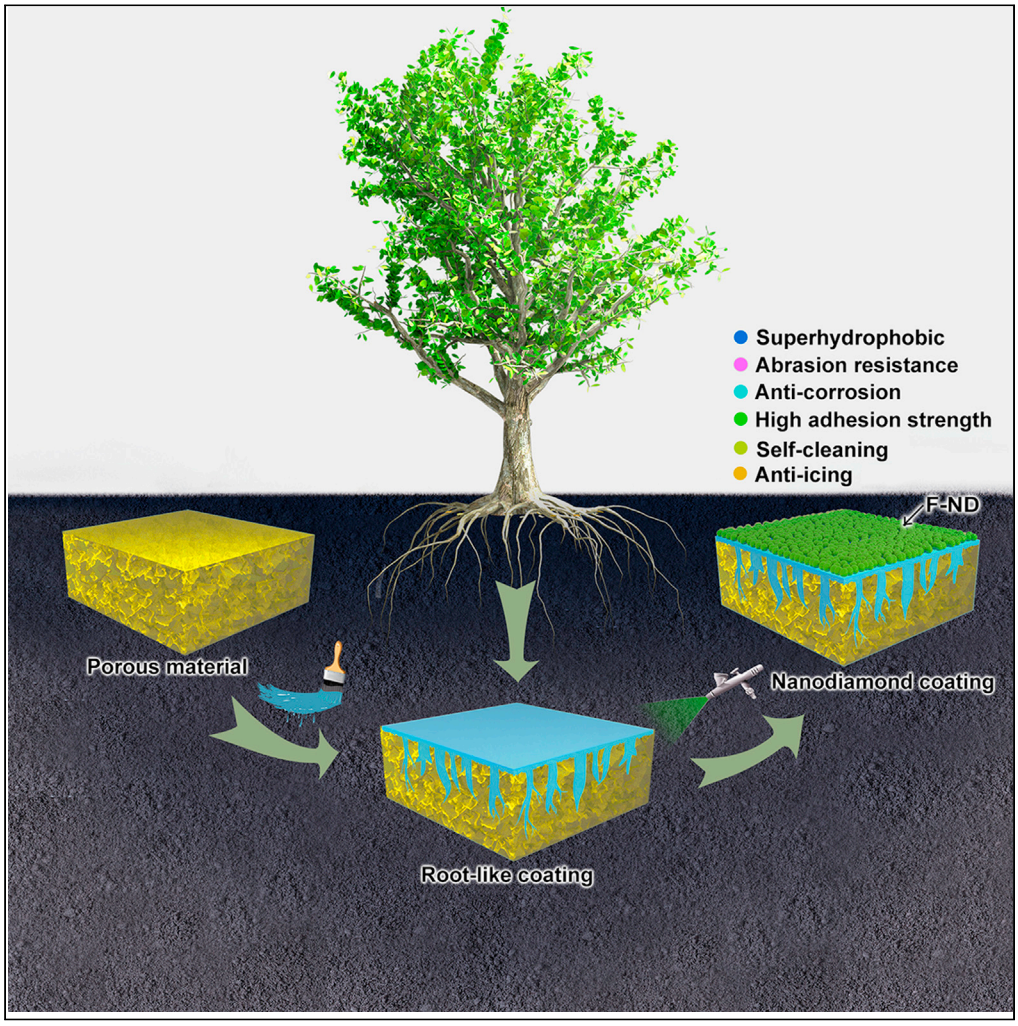

Guoliang Zhang, Qingyi Xie, Jinfeng Chi, Yuxian Chen, Hao Zheng, Chunfeng Ma, Guangzhao Zhang

msmcf@scut.edu.cn (C.M.)
msgzzhang@scut.edu.cn (G.Z.)

Highlights

A tree root-inspired superhydrophobic coating for porous structures was developed

The epoxy coating with high permeability can consolidate in pores and cracks

The ultra-hard fluorinated nanodiamonds provides remarkable abrasion-resistance

The surface has excellent self-cleaning, anti-icing, and anticorrosive abilities

Zhang et al., iScience *24*, 103197
October 22, 2021
https://doi.org/10.1016/j.isci.2021.103197

iScience

CellPress
OPEN ACCESS

Article

Tree root-inspired robust superhydrophobic coatings with high permeation for porous structures

Guoliang Zhang,[1,2] Qingyi Xie,[1,2] Jinfeng Chi,[1,2] Yuxian Chen,[1] Hao Zheng,[1] Chunfeng Ma,[1,3,*] and Guangzhao Zhang[1,*]

SUMMARY

Superhydrophobic coatings have tremendous potential for protecting porous structures from corrosion. However, the weak adhesion and poor abrasion resistance have long been challenges for their real-life applications. Inspired by tree roots, we prepared a robust superhydrophobic coating by spraying fluorinated nanodiamonds (FNDs) on a permeable epoxy coating. The epoxy can not only coat the surface but also permeate deeply inside a porous substrate and consolidate *in situ* as tree roots in soil. Thus, the structure is thoroughly reinforced where the pull-off strength reaches 9.4 MPa for concrete. On the other hand, the surface is covered with immobilized FNDs, forming a superhydrophobic surface. Thanks to the ultra-hard FNDs, the coating surface has high abrasion resistance and its superhydrophobicity holds even after 100 abrasion cycles. Moreover, it exhibits self-cleaning, anti-icing, and anticorrosion performance. It is promising in protecting various porous structures such as concrete, wood, and untreated corroded steel.

INTRODUCTION

Porous materials such as concrete, wood, and textiles are widely used in our life, where the porous structure often leads to corrosion. For example, concrete that has been used in roads, bridges, harbors, and other civil engineering projects suffers from corrosion in its service. Once Cl^-, SO_4^{2-}, and other ions permeate into its vacancy, they would cause corrosion of steel bars and salt crystallization swelling. These corrosive ions are carried by water with good penetrating property. Therefore, prevention of water ingress can effectively improve the durability of porous materials.

Superhydrophobic coatings with remarkable waterproof ability have received much attention for protecting porous structures and other facilities (Feng and Jiang, 2006; Gao and Jiang, 2004; Blossey, 2003; Lu et al., 2015; Jung et al., 2012; Zhang et al., 2008; She et al., 2013; Li et al., 2019; Xue et al., 2011). Generally, a superhydrophobic surface can be constructed with low-surface-energy materials with micro- and nanoscale architectures, where templating, spraying, etching, and electrochemical deposition have been used (Wang et al., 2016; Li et al., 2014; Gong et al., 2016; Xue et al., 2014a, 2014b; Tesler et al., 2015). However, the low-surface-energy materials weakly bond to the substrates, and thus the surface structures are readily damaged or corrosive. The weak adhesion and poor abrasion resistance become an obstacle to their large-scale applications. To solve the problems, adhesive layers were added, discrete microstructures were randomly introduced to bear abrasion, the surface structures were renewed, but the robustness was not significantly improved (Wang et al., 2020).

In nature, trees can grow and withstand the storms because their roots are deeply and tightly consolidated in soils. In this study, inspired by tree roots, a superhydrophobic coating has been prepared using fluorinated nanodiamonds (FNDs) and epoxy with reactive solvent of furfural and acetone (Scheme 1). The epoxy coating is first coated on porous structure (e.g., concrete), and FND suspension is sprayed on the incompletely cured epoxy to fabricate a superhydrophobic surface (designated as Ep-FND-S). The epoxy coating has high permeability so that it can penetrate small pores and cracks with size from about 0.1 to 10 μm in the substrate and consolidate *in situ* behaving like tree roots in soil reinforcing the concrete. On the other hand, the hydrophobic FNDs with ultra-high hardness are strongly adhered on the surface, which provides

[1]Faculty of Materials Science and Engineering, South China University of Technology, Guangzhou, China

[2]These authors contributed equally

[3]Lead contact

*Correspondence: msmcf@scut.edu.cn (C.M.), msgzzhang@scut.edu.cn (G.Z.)

https://doi.org/10.1016/j.isci.2021.103197

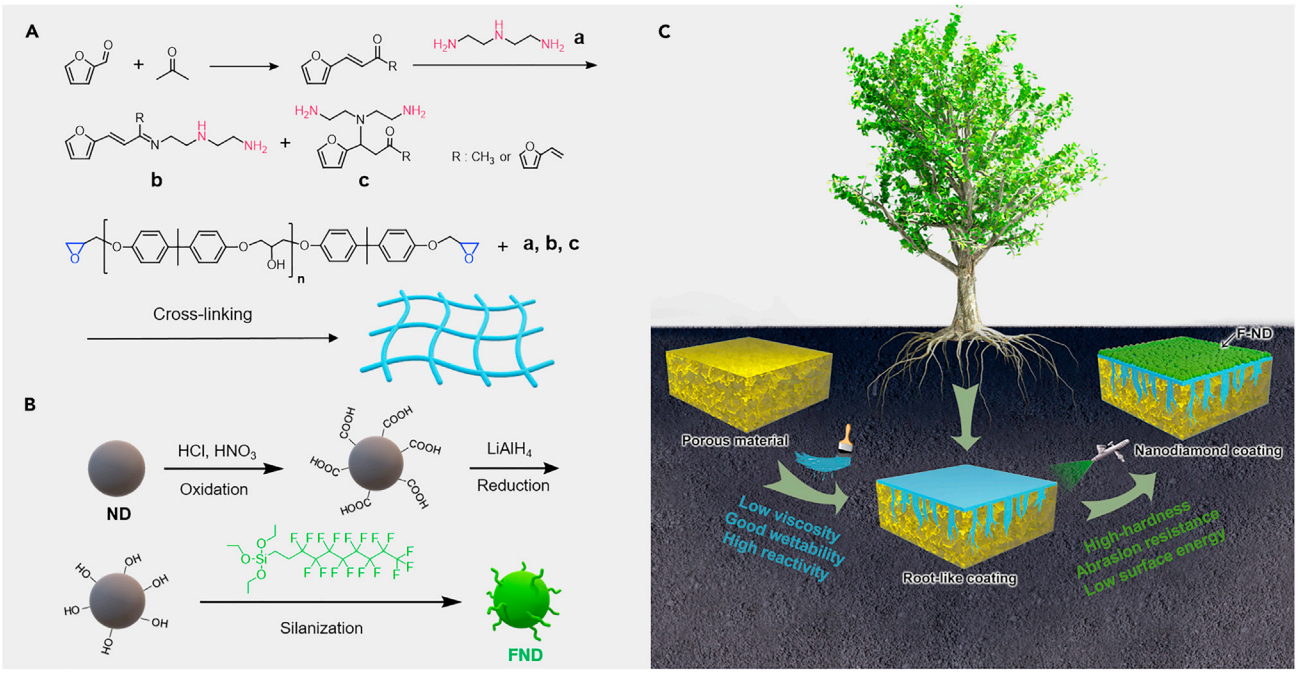

Scheme 1. Schematic of fabricating a robust superhydrophobic coating for a porous structure

(A) The reactions related to preparing the permeable epoxy coating.

(B) The preparation of fluorinated nanodiamond (FND).

(C) The procedures of preparing the superhydrophobic coating based on the permeable epoxy and FNDs.

the surface not only superhydrophobicity but also abrasion resistance. For comparison, a mixture of permeable coating and FND was applied directly on concrete (designated as Ep-FND-B), which hardly permeates inside owing to its high viscosity. The schematic illustration of the difference between the two materials is shown in Figure S1. The properties of coatings applied on mortar and other porous substrates were investigated. We attempt to develop a high-performance coating for reinforcement and protection of porous structures.

RESULTS

Morphology and chemical composition of the coating surface

The Fourier transform infrared spectroscopy, Raman spectroscopy, and scanning electron microscopy (SEM) results of FNDs are shown in Figure S2, demonstrating that FNDs with fluorinated groups and a particle size mostly ranging from 30 to 100 nm were successfully prepared.

Figure 1A shows the SEM images of the mortar surfaces with or without the coatings. The uncoated mortar (control) exhibits a rather rough surface with many microscale pores, whereas the mortar with the permeable epoxy coating (Ep) has a smooth surface. This is because the epoxy coating permeates into the pores of the mortar, forming a densely protective film on the surface. Some microbulges can be observed on the surface of epoxy coating previously mixed with FNDs (Ep-FND-B) in that they are not compatible. On the surface fabricated by spraying FND suspension on pre-coated epoxy (Ep-FND-S), many microscale protrusions are observed. They are micro- and nano-hierarchical structures formed by FNDs irregularly distributed on the surface.

The compositions of the coating surfaces were characterized by using energy-dispersive spectroscopy (EDS) combined with SEM, as shown in Figure 1B and Table S1. The mortar control mainly consists of C, O, Si, K, and Ca. Si comes from the cement and the standard sand used in mortar. On the mortar coated with Ep, C and O are found, whereas K, Ca, or Si is missing, indicating that the surface is completely covered by the epoxy coating. Unlike Ep, the Ep-FND-B contains F and Si, which are attributed to the presence of FND particles. Ep-FND-S has the same elements as Ep-FND-B. However, the latter has F and Si contents of

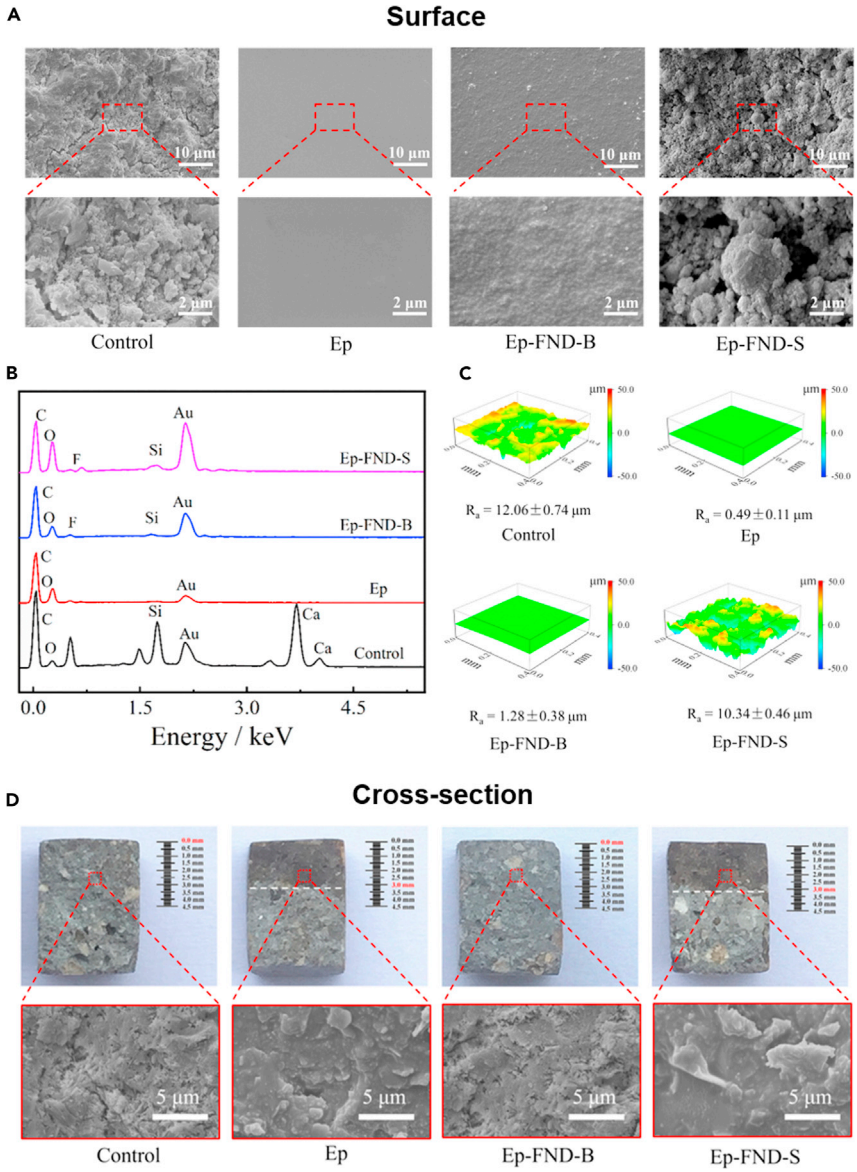

Figure 1. Morphology and elemental composition studies of mortar covered with different coatings

(A) The images of mortars surfaces observed with SEM.

(B) EDS spectra of the mortar surface.

(C) The images of mortars surfaces and the surface roughness obtained by a 3D profiler.

(D) The images of mortars cross sections observed with SEM.

17.11 and 1.62 wt%, respectively, much higher than those of the former (8.07 and 0.70 wt%, respectively), indicating the abundance of FNDs on the surface of Ep-FND-S.

Figure 1C shows the 3D topographies of the coating surfaces. The control sample is extremely rough with a surface roughness (Ra) of ~12.06 μm. Moreover, some peak-like structures can be observed. The topography of Ep surface is relatively flat with Ra of ~0.46 μm, indicating that the pores of the mortar are blocked by the epoxy coating. The Ep-FND-B surface has a relatively higher Ra (~1.28 μm) due to the presence of FNDs. Ep-FND-S has an Ra of ~10.34 μm and plenty of peak-like structures attributed to the aggregates of FNDs on the surface.

The cross-sectional morphologies were also examined (Figure 1D). A number of pores with different sizes can be observed in the control. However, the cross section no longer shows pores after coating with Ep.

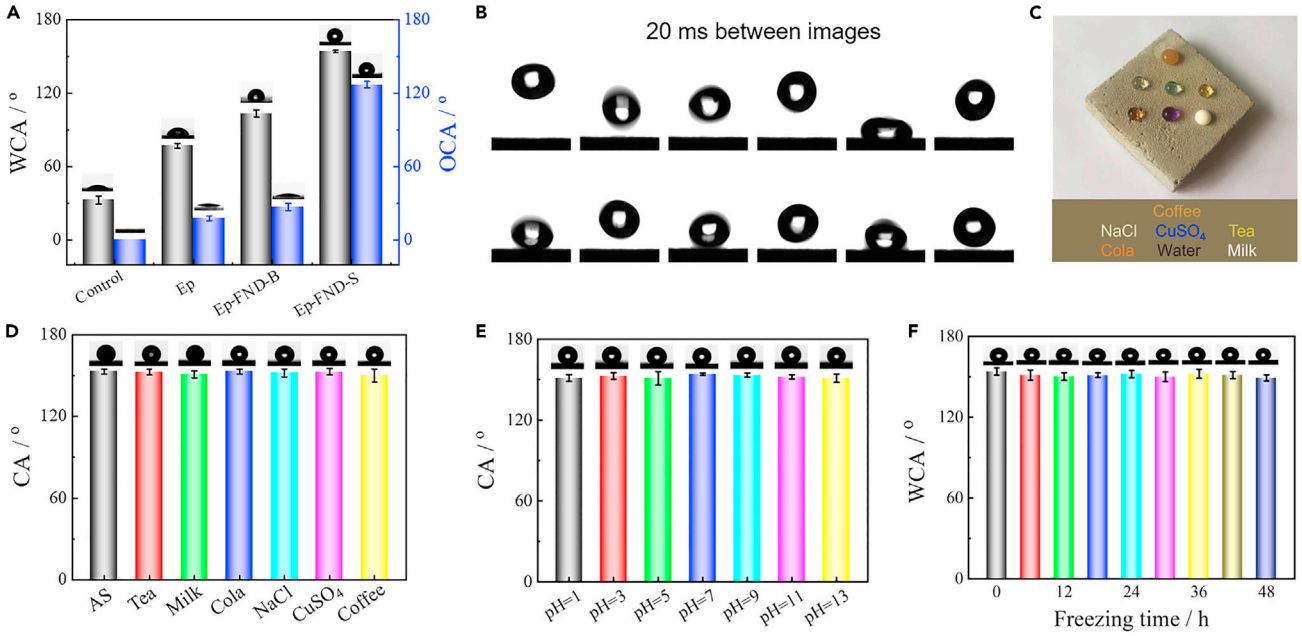

Figure 2. The superhydrophocity of the coatings

(A) Water contact angles (WCAs) and oil contact angles (OCAs) of the surfaces.

(B) High-speed camera images of bouncing process of a 10-μL water droplet falling on the Ep-FND-S coating.

(C) An image of some common liquids on the surfaces.

(D) Contact angles (CAs) of common liquids on the surfaces, where the AS is artificial seawater.

(E) Contact angles (CAs) of liquids of different pH on the surfaces.

(F) WCAs of the surfaces after being frozen at −15°C for different durations. The scale bar is the standard deviation.

This clearly shows the coating not only covers the surface but also permeates into the pores or defects in the mortar. In this system, furfural and acetone do not serve only as the diluent of epoxy. Instead, they can act as reactive solvents and chemically link with epoxy via amine. As a result, the Ep coating has low viscosity of 6 mPa·s and excellent wettability for mortar (Zhang et al., 2018), so it not only covers the surface but also permeates into the pores or defects in the mortar. Actually, the permeation depth is about 3.0 mm. The surface coated with Ep-FND-B still has many pores like the control. This is because it has significantly increased viscosity (410 mPa·s) and decreased wettability in the presence of the hydrophobic FNDs, thereby preventing the epoxy from permeating the mortar. This is further confirmed by EDS spectra of cross section of mortar coated by Ep-FND-B (Figure S3 and Table S2), where F cannot be detected in the mortar area. Since the Ep-FND-S surface was prepared by coating the mortar with Ep and then spraying FNDs on the incompletely cured Ep, it has a cross-sectional morphology and a permeation depth close to those for the Ep surface. EDS linear scan was performed on the cross section of the samples with varying depth (Figure S4).

The above measurements clearly demonstrate that the epoxy coating can permeate the porous mortar and blocks the pores, while most sprayed FNDs cover the surface forming a surface with micro- and nanostructures, which increases the hydrophobicity.

The wettability of the coatings

Figure 2A shows the contact angles (CAs) of the coatings for water and oil (hexadecane). The control has a water contact angle (WCA) of 32°. As oil was dropped onto the surface, it quickly spread and permeated the mortar. Hence, the oil contact angle (OCA) is defined as 0° due to the porous structure of the mortar. Ep coating has a WCA of 77° and an OCA of 18°. The former is higher than that of the control because the coating effectively inhibited the spread of water and oil. Owing to the good water repellence of fluoro groups on FNDs (Xie et al., 2020), the Ep-FND-B coating has a WCA and OCA of 103° and 27°, respectively, higher than those for Ep. Ep-FND-S has a WCA and an OCA of 154° and 126°, respectively. These facts indicate that the coated surface has hydrophobicity and oleophobicity.

For a coating to be classified as superhydrophobic, it should have a high WCA (>150°) and low friction and adhesion to water droplets. Video S1 shows the rolling-off process of water on the superhydrophobic coating. When the substrate was inclined at an angle of 4.5°, the water droplets began to roll off the surface, indicating that Ep-FND-S has a roll-off angle of 4.5°. Figure 2B shows that the water droplets underwent a repeated "bouncing process" as they cascaded down the surface, and they maintained a nearly spherical shape on the surface while falling on the surface from a height of 3 cm. Figure S5 presents the entire bouncing process. Clearly, the surface coated with Ep-FND-S has extremely low adhesion to water droplets. When Ep-FND-S was immersed in water, a silver mirror phenomenon was observed (Figure S6), further indicating the superhydrophobicity since the air layer around a superhydrophobic surface in water can cause such a phenomenon (Huang et al., 2015).

The wettability of a superhydrophobic surface can be interpreted using the Cassie-Baxter theory (Cassie and Baxter, 1945). On the mortar coated with Ep-FND-S, the pores and cavities between micro- and nanoscale protrusions caused by the FNDs can trap air forming a protective layer that effectively decreases the contact area between the substrate and water. Namely, the surface contains a solid-air-water interface, significantly increasing the resistance of the surface to water. Moreover, the perfluorodecyltriethoxysilane groups on FNDs further reduce the surface energy of the coating. In terms of the Cassie-Baxter equation, $\cos\theta_1 = f_{sl}\cos\theta_2 + f_{sl} - 1$, where θ_1 and θ_2 are the WCAs of the superhydrophobic coating and mortar, respectively, and f_{sl} is the fraction of the contact area between the water droplet and the solid surface. For Ep-FND-S coating, since θ_1 = 154° and θ_2 = 32° (Figure 2A), f_{sl} is 0.055. This low value of f_{sl} indicates that the contact area between the water droplets and the superhydrophobic surface is about 5.5%. Thus, 94.5% of the surface is in contact with air. This small amount of contact with the surface allows the water to maintain a nearly spherical shape on the surface of Ep-FND-S, so the surface is superhydrophobic.

The Ep-FND-S-coated surface was then contaminated by different liquids to test its self-cleaning property. The contamination not only has negative effect on the aesthetics of a coating but also destroys its protective function. In this test, 3.5 wt% NaCl solution, cola, coffee, milk, tea, artificial seawater, and $CuSO_4$ solution were applied to investigate the surface repellency of the coating (Figure 2C). The CAs on Ep-FND-S are shown in Figure 2D. Clearly, a little difference between the liquids can be observed, and they are nearly spherical with CAs over 150°. Similarly, mud cannot adhere to the Ep-FND-S coating (Video S2). The superhydrophobic Ep-FND-S coating has outstanding repellency to various contaminants.

Figure 2E shows pH dependence of the CAs of droplets on Ep-FND-S surfaces. The CAs slightly vary from about 151° to 154°, and the small difference is attributed to the air trapped by the micro- and nanostructures acting as a barrier that effectively decreases the contact area between the surface and the droplets. Moreover, the CAs are all higher than 150° in the range pH 1–13, indicating that Ep-FND-S has chemical stability. Figure 2F shows the WCAs of Ep-FND-S surfaces after they are placed in a freezer with different durations at −15°C. The WCAs range from 150° to 154°, and the water droplets maintain spherical shape on the surface (inset of Figure 2F). Clearly, the Ep-FND-S surface has good resistance to freezing and can be used at a low temperature.

The mechanical properties of the coatings

Mechanical durability is critical for a coating. Figure 3A shows the bonding strength of the coating to the mortar and the failure mode of the coated mortar. The control sample has a pull-off strength of 4.1 MPa. The mortar specimen coated with Ep has a pull-off strength of 9.4 MPa, and failure occurred in the mortar brick, indicating that the mortar was remarkably reinforced. This is because the epoxy is not only coated on the mortar surface but also permeates into pores and consolidates there forming a robust epoxy-mortar composite as tree roots in soil. The reactive solvents furfural and acetone play a contributive role here. Conventional unreactive solvents vaporize from the pores during or after curing, leading to some incompletely blocked pores and defects of concrete. The solvents here chemically cross-link with epoxy via amine, so it significantly dilutes the epoxy without causing defects. As a result, the Ep coating can permeate deeply into the concrete and consolidate *in situ* (Zhang et al., 2018). In contrast, when the mortar is coated with polystyrene (PS) that is commonly used as adhesive in superhydrophobic coatings (Xue et al., 2014a, 2014b; Latthe and Demirel, 2013), the strength almost did not change compared with the control. This is because PS cannot permeate into the mortar but is merely covered on the surface. Besides, it only contains nonpolar groups that weakly interacted with the mortar. Accordingly, the permeation allows epoxy coating to improve its adhesion.

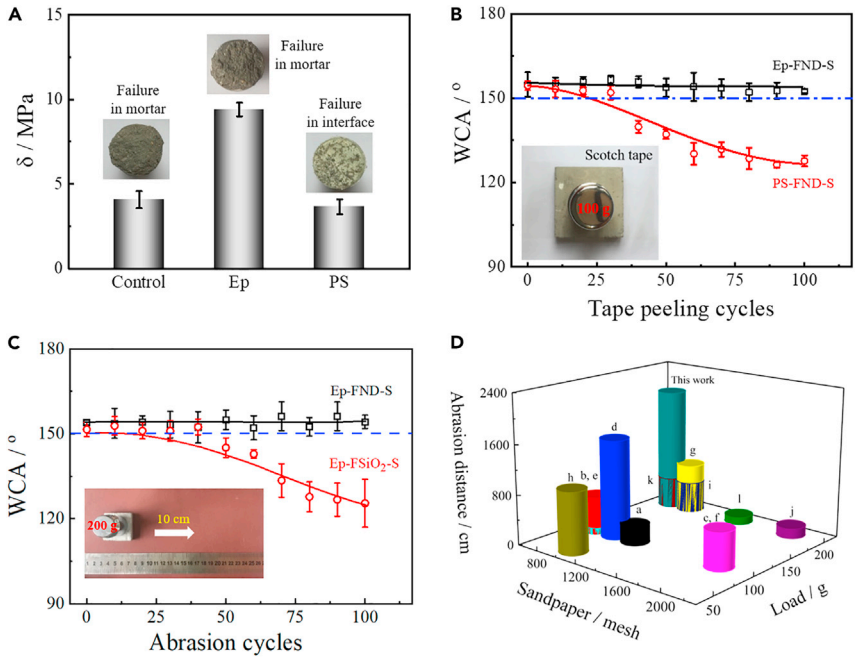

Figure 3. Mechanical robustness of the coatings

(A) Pull-off strength and failure modes of mortars coated with permeable epoxy and polystyrene (PS) coatings.

(B) WCA of the coatings after multiple peeling tests with adhesive tape, where the inset shows that the image of tape peeling test.

(C) WCA of the coatings after different abrasion cycles, where the inset shows that the image of the sandpaper abrasion test.

(D) Comparison of abrasion resistance of Ep-FND-S coating with other superhydrophobic coatings reported in the references (a: Long et al., 2017; b: Ye et al., 2017; c: Zhou et al., 2017; d: Zhang et al., 2019; e: Peng et al., 2019; f: Zhou et al., 2019; g: Sun et al., 2019; h: Liu et al., 2017; i: Wang et al., 2017a, 2017b; j: Guo et al., 2016; k: Guo et al., 2017; l: Huang et al., 2018). The scale bar is the standard deviation.

Figure 3B shows the WCA as a function of tape-peeling times. The Ep-FND-S coating could resist at least 100 tape-peeling cycles with almost no decrease in WCA. This is because FNDs are strongly adhered by epoxy, thus maintaining its surface composition and micro-/nanostructures. In contrast, for the PS-FND-S coating with PS as adhesive, WCA decreases as the peeling cycle increases, and it dropped to 127° after 100 cycles (Figure S7). This is because the nonpolar PS is not able to firmly adhere FNDs on the surface.

A sandpaper abrasion test was used to evaluate the mechanical durability of the coatings (Wang et al., 2017a, 2017b). Figure 3C shows the WCA as a function of the number of abrasion cycles. After abrasion, the superhydrophobic Ep-FSiO$_2$-S coating prepared by spraying fluorinated SiO$_2$ on permeable epoxy decreases from 150° to 125° in WCA. However, the WCA on Ep-FND-S surface only slightly decreased from 156° to 152°. That is, the superhydrophobicity holds even after 100 sandpaper abrasion cycles. Actually, the surface still exhibits micro- and nano structures, which slightly changes after such treatments, and the water droplets can still bounce on it. The FNDs on surface contribute significantly to the abrasion resistance, as nanodiamonds have extremely high hardness. Actually, Ep-FND-S has superior abrasion resistance, as its superhydrophobicity is maintained upon the lowest mesh (800 meshes, the roughest), longest abrasion distance (2000 cm), and largest load (200 g) among the studies of robust superhydrophobic coatings (Figure 3D).

The protective performances and versatility of the coatings

Figure 4A shows self-cleaning property of the coatings. Water droplets easily rolled off the Ep-FND-S surface, thus carrying away the yellow pigment and leaving a distinct rolling trace. As water was further dropped, the pigment was completely carried away, and a clean surface was recovered. This is attributed to the solid-air-water interface that remarkably increases the resistance of the Ep-FND-S surface to water (illustrated in Figure S8). However, the other surfaces were still fouled by the pigment since they have relatively low WCA (Figure 1A). Therefore, these surfaces can be wet by the water droplets.

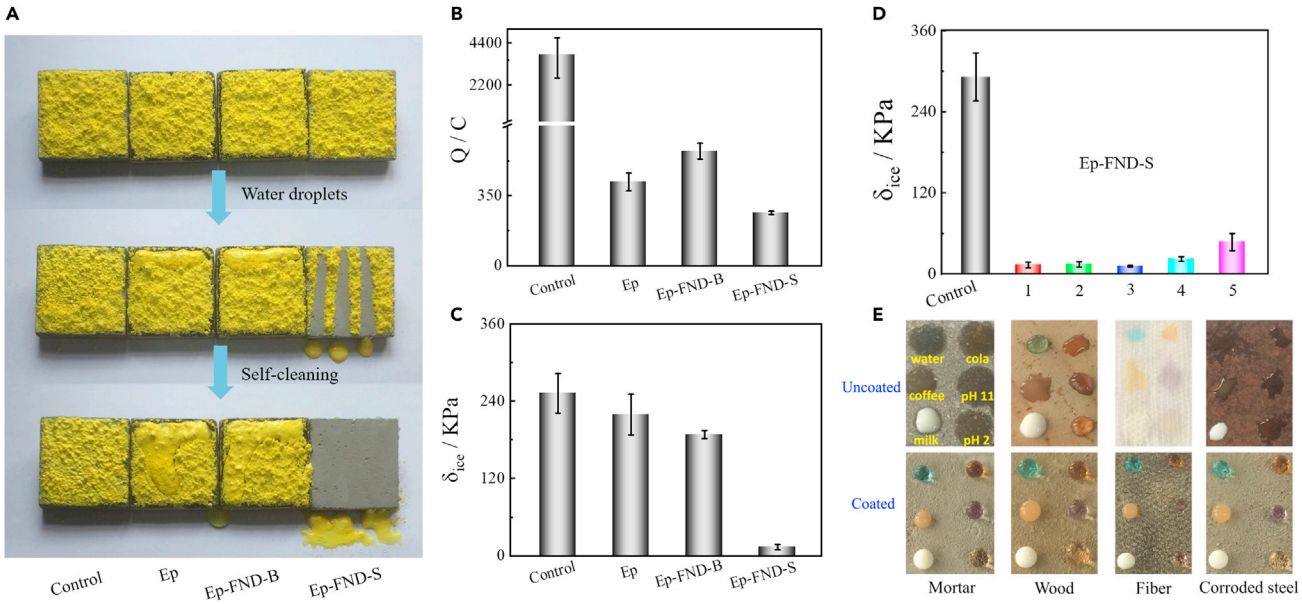

Figure 4. The comprehensive protective performances of the coatings

(A) Images of yellow pigment on different coatings washed by water droplets, where the coated mortars were tilted at 45°.

(B) Total charge (Q) allowed to pass by the coated mortars. The experiment was conducted according to ASTM C1202.

(C) Adhesion strength of icicles on the mortars coated with different coatings.

(D) The adhesion strength of icicles on Ep-FND-S coating after different icing/deicing cycles, with uncoated mortar before the cycle as control.

(E) Images of some liquids on mortars with or without coated Ep-FND-S superhydrophobic coating. The scale bar is the standard deviation.

The anticorrosion properties of the coatings were studied by chloride resistance test (Figure 4B). The uncoated mortar control allowed 3600 C of charge, indicating it readily suffers from corrosion. Ep coating only allowed a total charge of 418 C, much lower than that of the control. This is because the epoxy coating permeated into concrete and blocked the pores and defects in the concrete (Figure 1D), thereby effectively impeding the ingress of chloride. Ep-FND-B allowed a higher total charge than Ep because it cannot permeate the concrete. Ep-FND-S allowed the lowest total charge of 264 C. This is because air layer captured by the micro- and nanoscale protrusions acted as a barrier that remarkably decreased the contact area between the substrate and the corrosive ions. On the other hand, the epoxy can permeate the concrete and repair the defects, further inhibiting the ingress of corrosive ions.

Figure 4C shows the anti-icing properties of the coatings. The mortar control has the highest ice adhesion strength of 252.5 kPa. This is understandable because the sample formed an "anchor structure" composed of embedded ice at a temperature below 0°C owing to the permeation of water, which greatly increased the bond strength of the ice (Figure S9) (Peng et al., 2018). The Ep coating has an ice adhesion strength of 219.3 kPa. The epoxy formed a dense, smooth film on the surface of the substrate, thereby impeding the permeation of water into the substrate. The Ep-FND-B coating has an ice adhesion strength of 188.4 kPa, lower than that of Ep coating. The Ep-FND-S coating has the lowest ice adhesion strength of 13.3 kPa, 94% lower than that of the control. This is because the air captured by the micro- and nanostructures significantly reduced the contact between the ice and the mortar surface. Moreover, the strain force generated by the air pockets owing to squeezing by the surrounding ice reduced the ice adhesion strength (Shen et al., 2018; Fu et al., 2014). Anyhow, the Ep-FND-S coating exhibits the best anti-icing performance. Icing/deicing cycle experiments on the Ep-FND-S coating were also conducted to evaluate its ice-phobic durability (Figure 4D). Although the adhesion strength slightly increased with the number of icing/deicing cycles, it is remarkably lower than that of the control, demonstrating the durable anti-icing performance of the coating.

The fabricated superhydrophobic coating is not specific to concrete or mortar; it can also be applied to other porous structures such as wood, gauze, and corroded steel plates. Figure 4E shows that coffee, cola, acid, base, milk, and water can easily spread on the surface of the uncoated porous structures and even permeate them. However, the droplets maintain a nearly spherical shape on the porous structures covered with the superhydrophobic Ep-FND-S coating. Therefore, the superhydrophobic coating can protect various porous structures

from corrosion and contamination so that their service life is extended. The liquids are common in daily life or industry. Although they have different properties such as pH and wettability, while the porous structures have different pore types and sizes, the coating is effective for all these cases, demonstrating its versatility.

DISCUSSION

Inspired by tree roots, a robust superhydrophobic coating Ep-FND-S with self-cleaning, anti-icing, and anti-corrosion properties has been fabricated to protect porous structures by a facile method. The permeable epoxy can penetrate into concrete and consolidate *in situ*, forming an epoxy-concrete composite. This is further supported by EDS linear scan spectra and cross-sectional morphologies of mortar coated with Ep-FND-S (Figure S4). At the cross section of mortar, Si can be detected owing to its existence in the cement and standard sand that do not contain any F. For Ep, F is undetected, and Si is only detected beyond ~50 μm, because the region of 0–50 μm consists of the epoxy coating and the region beyond 50 μm consists of the coating/mortar composite layer. As to Ep-FND-B, although F and Si should theoretically be detected in the coating, none was observed. This is because FNDs were embedded by the epoxy. F is observed in the upper layer of Ep-FND-S, and the F content gradually decreases to zero as the depth increases, indicating that the sprayed FNDs are only partly deposited in the epoxy, but mostly on surface. As a result, the concrete is significantly reinforced by the epoxy, where the adhesion strength between the concrete and epoxy is 9.4 MPa, two times higher than that of mortar control. FNDs fixed on the surface form a superhydrophobic surface with micro- and nanostructures, and it has a higher WCA (154°) and a lower sliding angle (4.5°). FNDs with superior hardness makes the surface with excellent mechanical performance possible. Ep-FND-S holds superhydrophobicity after harsh abrasion for 100 times, indicating remarkable mechanical robustness. Moreover, the coating is also able to resist cold, various contaminants, and corrosive ions.

Ep-FND-S is a versatile protective coating not only for concrete but also for a variety of porous structures and objects including wood, fiber, and even untreated corroded steel. It is readily prepared by spraying nanoparticle suspension on brushed coating. The coating is promising to find applications in several fields.

Limitations of the study

Apart from the above breakthroughs, there are a few limitations in this study. In principle, other hard nano-fillers may also be used to fabricate such enduring superhydrophobic coatings, and this work focuses on nanodiamond. It would be interesting to utilize hard nano-fillers with other structures (e.g., layer and tube structures) and sizes. In addition, the superhydrophobic coating was prepared by a two-step (coat-spray) method in this work. It would be possible to use a one-step process if the permeation of epoxy coating can be further tuned. These will be explored in the future.

STAR★METHODS

Detailed methods are provided in the online version of this paper and include the following:

- KEY RESOURCES TABLE
- RESOURCE AVAILABILITY
  - Lead contact
  - Materials availability
  - Data and code availability
- METHOD DETAILS
  - Preparation of fluorinated nano-diamonds (FNDs)
  - Preparation of fluorinated SiO_2 nanoparticles ($FSiO_2$)
  - Preparation of the coating containing nanoparticles
  - Characterization

SUPPLEMENTAL INFORMATION

Supplemental information can be found online at https://doi.org/10.1016/j.isci.2021.103197.

ACKNOWLEDGMENTS

The financial support of National Natural Science Foundation of China (52003082), the Opening Project of Guangdong Provincial Key Laboratory of Technique and Equipment for Macromolecular Advanced Manufacturing (2019KFKT05), and China Postdoctoral Science Foundation (2019M662904) is acknowledged.

AUTHOR CONTRIBUTIONS

Guangzhao Zhang and C.M. designed the experiments and analyzed the results. Guoliang Zhang, Q.X., and J.C. carried out the experiments, interpreted the results, and prepared the manuscript. All authors contributed to editing the manuscript.

DECLARATION OF INTERESTS

The authors declare no conflict of interest.

Received: July 1, 2021
Revised: September 6, 2021
Accepted: September 24, 2021
Published: October 22, 2021

REFERENCES

Blossey, R. (2003). Self-cleaning surfaces-virtual realities. Nat. Mater. *2*, 301–306.

Cassie, A.B.D., and Baxter, S. (1945). Large contact angles of plant and animal surfaces. Nature *155*, 21–22.

Chi, J.F., Zhang, G.L., Xie, Q.Y., Ma, C.F., and Zhang, G.Z. (2020). High performance epoxy coating with cross-linkable solvent via Diels-Alder reaction for anti-corrosion of concrete. Prog. Org. Coat. *139*, 105473.

Feng, X.J., and Jiang, L. (2006). Design and creation of superwetting/antiwetting surfaces. Adv. Mater. *18*, 3063–3078.

Fu, Q.T., Wu, X.H., Kumar, D., Ho, J.W.C., Kanhere, P.D., Srikanth, N., Liu, E.J., Wilson, P., and Chen, Z. (2014). Development of sol–gel icephobic coatings, effect of surface roughness and surface energy. ACS. Appl. Mater. Inter. *6*, 20685–20692.

Gao, X.F., and Jiang, L. (2004). Biophysics: water-repellent legs of water striders. Nature *432*, 36.

Gong, D.W., Long, J.Y., Jiang, D.F., Fan, P.X., Zhang, H.J., Li, L., and Zhong, M.L. (2016). Robust and stable transparent superhydrophobic polydimethylsiloxane films by duplicating via a femtosecond laser-ablated template. ACS Appl. Mater. Inter. *8*, 17511–17518.

Guo, F., Wen, Q.Y., Peng, Y.B., and Guo, Z.G. (2017). Simple one-pot approach toward robust and boiling-water resistant super-hydrophobic cotton fabric and the application in oil/water separation. J. Mater. Chem. A. *5*, 21866–21874.

Guo, J., Yang, F.C., and Guo, Z.G. (2016). Fabrication of stable and durable super-hydrophobic surface on copper substrates for oil-water separation and ice-over delay. J. Colloid Interf. Sci. *466*, 36–43.

Huang, J.D., Wang, S.Q., Lyu, S.Y., and Fu, F. (2018). Preparation of a robust cellulose nanocrystal super-hydrophobic coating for self-cleaning and oil-water separation only by spraying. Ind. Crop Prod. *122*, 438–447.

Huang, J.Y., Li, S.H., Ge, M.Z., Wang, L.N., Xing, T.L., Chen, G.Q., Liu, X.F., Al-Deyab, S.S., Zhang, K.Q., Chen, T., and Lai, Y.K. (2015). Robust superhydrophobic TiO2@fabrics for UV shielding, self-cleaning and oil–water separation. J. Mater. Chem. A. *3*, 2825–2832.

Jung, S., Tiwari, M.K., Doan, N.V., and amd Poulikakos, D. (2012). Mechanism of supercooled droplet freezing on surfaces. Nat. Commun. *3*, 615.

Latthe, S.S., and Demirel, A.L. (2013). Polystyrene/octadecyltrichlorosilane superhydrophobic coatings with hierarchical morphology. Polym. Chem. *4*, 246–249.

Li, M., Bian, C., Yang, G.X., and Qiang, X.H. (2019). Facile fabrication of water-based and non-fluorinated superhydrophobic sponge for efficient separation of immiscible oil/water mixture and water-in-oil emulsion. Chem. Eng. J. *368*, 350–358.

Li, Y., Chen, S.S., Wu, M.C., and Sun, J.Q. (2014). All spraying Processes for the fabrication of robust, self-healing, superhydrophobic coatings. Adv. Mater. *26*, 3344–3348.

Liu, M.M., Hou, Y.Y., Li, J., Tie, L., Peng, Y.B., and Guo, Z.G. (2017). Inorganic adhesives for robust, self-healing, super-hydrophobic surfaces. J. Mater. Chem. A. *5*, 19297–19305.

Long, M.Y., Peng, S., Deng, W.S., Miao, X.R., Wen, N., Zhou, Q.N., Yang, X.J., and Deng, W.L. (2017). A robust super-hydrophobic PDMS@ZnSn(OH)6 coating with under-oil self-cleaning and flame retardancy. J. Mater. Chem. A. *5*, 22761–22771.

Lu, Y., Sathasivam, S., Song, J.L., Crick, C.R., Carmalt, C.J., and Parkin, I.P. (2015). Robust self-cleaning surfaces that function when exposed to either air or oil. Science *347*, 1132–1135.

Peng, C., Zhang, H., You, Z.P., Xu, F., Jiang, G.S., Lv, S.T., Zhang, R., and Yang, H. (2018). Preparation and anti-icing properties of a superhydrophobic silicone coating on asphalt mixture. Constr. Build. Mater. *189*, 227–235.

Peng, J.Y., Zhao, X.J., Wang, W.F., and Gong, X. (2019). Durable self-cleaning surfaces with super-hydrophobic and highly oleophobic properties. Langmuir *35*, 8404–8412.

She, Z.X., Li, Q., Wang, Z.W., Li, L.Q., Chen, F.N., and Zhou, J.C. (2013). Researching the fabrication of anticorrosion superhydrophobic surface on magnesium alloy and its mechanical stability and durability. Chem. Eng. J. *228*, 415–424.

Shen, Y.Z., Wu, Y., Tao, J., Zhu, C.L., Chen, H.F., Wu, Z.W., and Xie, Y.H. (2018). Spraying fabrication of durable and transparent coatings for anti-icing application, dynamic water repellency, icing delay, and ice adhesion. ACS. Appl. Mater. Inter. *11*, 3590–3598.

Sun, R.Y., Zhao, J., Li, Z., Mo, J.L., Pan, Y.J., and Luo, D.B. (2019). Preparation of mechanically durable superhydrophobic aluminum surface by sandblasting and chemical modification. Prog. Org. Coat. *133*, 77–84.

Tesler, A.B., Kim, P., Kolle, S., Howell, C., Ahanotu, O., and Aizenberg, J. (2015). Extremely durable biofouling-resistant metallic surfaces based on electrodeposited nanoporous tungstite films on steel. Nat. Commun. *6*, 8649.

Wang, D.H., Sun, Q.Q., Hokkanen, M.J., Zhang, C.L., Lin, F.Y., Liu, Q., Zhu, S.P., Zhou, T.F., Chang, Q., He, B., et al. (2020). Design of robust superhydrophobic surfaces. Nature *582*, 55–59.

Wang, L., Gong, Q.H., Zhan, S.H., Jiang, L., and Zheng, Y.M. (2016). Robust anti-icing performance of a flexible superhydrophobic surface. Adv. Mater. *28*, 7729–7735.

Wang, P., Sun, B., Yao, T., Chen, M.J., Fan, X.L., Han, H.L., Li, L., and Wang, C. (2017a). A novel dissolution and resolidification method for preparing robust superhydrophobic polystyrene/silica composite. Chem. Eng. J. *326*, 1066–1073.

Wang, S.L., Yu, X.Q., and Zhang, Y.F. (2017b). Large-scale fabrication of translucent, stretchable and durable super-hydrophobic composite films. J. Mater. Chem. A. *5*, 23489–23496.

Xie, Q.Y., Liu, C., Lin, X.B., Ma, C.F., and Zhang, G.Z. (2020). Nanodiamond reinforced poly(dimethylsiloxane)-based polyurea with self-healing ability for fouling release coating. ACS Appl. Polym. Mater. *2*, 3181–3188.

Xue, C.H., Li, Y.R., Zhang, P., Ma, J.Z., and Jia, S.T. (2014a). Washable and wear-resistant superhydrophobic surfaces with self-cleaning property by chemical etching of fibers and hydrophobization. ACS Appl. Mater. Inter. *6*, 10153–10161.

Xue, C.H., Zhang, Z.D., Zhang, J., and Jia, S.T. (2014b). Lasting and self-healing superhydrophobic surfaces by coating of polystyrene/SiO2 nanoparticles and polydimethylsiloxane. J. Mater. Chem. A. *2*, 15001–15007.

Xue, Z.X., Wang, S.T., Lin, L., Chen, L., Liu, M.J., Feng, L., and Jiang, L. (2011). A novel superhydrophilic and underwater superoleophobic hydrogel-coated mesh for oil/water separation. Adv. Mater. *23*, 4270–4273.

Ye, H., Zhu, L.Q., Li, W.P., Liu, H.C., and Chen, H.N. (2017). Constructing fluorine-free and cost-effective super-hydrophobic surface with normal-alcohol-modified hydrophobic SiO2 nanoparticles. ACS Appl. Mater. Inter. *9*, 858–867.

Zhang, F.Z., Zhao, L.L., Chen, H.Y., Xu, S.L., Evans, D.G., and Duan, X. (2008). Corrosion resistance of superhydrophobic layered double hydroxide films on aluminum. Angew. Chem. Int. Ed. *120*, 2500–2503.

Zhang, G.L., Xie, Q.Y., Ma, C.F., and Zhang, G.Z. (2018). Permeable epoxy coating with reactive solvent for anticorrosion of concrete. Prog. Org. Coat. *117*, 29–34.

Zhang, Y.F., Zhang, L.Q., Xiao, Z., Wang, S.L., and Yu, X.Q. (2019). Fabrication of robust and repairable super-hydrophobic coatings by an immersion method. Chem. Eng. J. *369*, 1–7.

Zhou, C.L., Chen, Z.D., Yang, H., Hou, K., Zeng, X.J., Zheng, Y.F., and Cheng, J. (2017). Nature-inspired strategy toward super-hydrophobic fabrics for versatile oil/water separation. ACS Appl. Mater. Interfaecs. *9*, 9184–9194.

Zhou, X., Yu, S.R., Wang, J., Zang, J., and Lv, Z.X. (2019). Superhydrophilic anti-corrosive and super-hydrophobic durable TiO2/Ti mesh for oil/water separation. J. Taiwan Inst. Chem. E. *105*, 124–133.

STAR★METHODS

KEY RESOURCES TABLE

REAGENT or RESOURCE	SOURCE	IDENTIFIER
Chemicals, peptides, and recombinant proteins		
Diglycidyl ether of bisphenol A (DGEBA) with epoxide equivalent weight (EEW) of 180–190 g/equiv	Nantong Xingchen Synthetic Material Co., China	CAS: 1675-54-3
Nanodiamonds (NDs)	Hebei Wei Xing Chemical Co., China.	CAS: 7782-40-3
1H-, 1H-, 2H-, and 2H-perfluorodecyltriethoxy-silane (PFDTES)	Zhejiang Chemical Industry Research Institute Co., China.	CAS: 101947-16-4
2,4,6-tris-(dimethylamino-methyl) phenol (DMP-30)	Guangzhou Chem. Reagent Co., China	CAS: 90-72-2
furfural	Guangzhou Chem. Reagent Co., China	CAS: 98-01-1
Other		
Scanning electron microscope	Zeiss, Pro G3, Germany	https://www.zeiss.com/microscopy/int/products/scanning-electron-microscopes.html
Theta Auto 113	KSV, Biolin	https://www.biolinchina.com/product/theta-series-technical-indicators
OCA50	Dataphysics	http://www.dataphys.com.cn/pro_content.aspx?id=103&mid=29
NEL-PDR concrete permeability tester	Naier, China	https://www.hi1718.com/product/2014220115640425.html
PosiTest AT-A pull-off adhesion tester	DeFelsko, USA	https://www.defelsko.com/positest-at

RESOURCE AVAILABILITY

Lead contact

Further information and requests for resources should be directed to and will be fulfilled by the lead contact, Chunfeng Ma (msmcf@scut.edu.cn).

Materials availability

All materials generated in this study are available from the lead contact without restriction.

Data and code availability

- All data used in the study are included in this publication and would be made available upon request.
- Any additional information required to reanalyze the data reported in this paper is available from the lead contact upon request.
- This paper does not report original code.

METHOD DETAILS

Preparation of fluorinated nano-diamonds (FNDs)

FNDs were prepared through three steps: oxidation, reduction, and silanization, as described elsewhere (Xie et al., 2020). The oxidation reaction was conducted to generate hydroxyl and carboxylic groups on the ND surface. Afterward, the carboxylic groups were reduced to hydroxyl groups so that abundant hydroxyl groups would be present for silanization. The silanization of PFDTES and hydroxyl immobilized the perfluoro groups on the ND surface. The obtained FNDs have a diameter of 30–100 nm.

Preparation of fluorinated SiO_2 nanoparticles ($FSiO_2$)

The surface of SiO_2 was also modified with perfluoro groups by silanization. Then, 4.0 g of SiO_2 nanoparticles were added into 120 mL of absolute ethanol, and the mixture was stirred for 30 min at room

temperature. Afterward, 1.0 g of PFDTES was added to the system, which was then heated to 75°C for 3 h in an argon atmosphere. The nanoparticles were collected through centrifugation and vacuum-dried at 40°C for 24 h. The $FSiO_2$ suspension was prepared by dispersing 1.0 g of $FSiO_2$ into 9.0 g of an acetone–ethanol (3/1, v/v) mixture and stirring the mixture for 2 h at 25°C.

Preparation of the coating containing nanoparticles

The permeable epoxy coatings were prepared as shown in Figure 1, following methods presented in the literature (Zhang et al., 2018). The coating used as the adhesive (0.64 g) was brushed onto the substrate with an area of 4 cm × 4 cm. As the coating cured for 4 h at room temperature, 3.0 g of the FND suspension (10 wt% in acetone) was sprayed on the precoated permeable epoxy coating. The distance between the spray gun and substrate was ~10 cm. Then, the coating was further cured at room temperature for 14 d prior to testing. This coating was named Ep-FND-S. Similarly, the coating with PS and FND (PS-FND-S) and the coating with permeable epoxy and $FSiO_2$ (Ep-$FSiO_2$-S) were prepared via the same procedure, except for the use of adhesive or nanoparticles. For comparison, mortar was also coated with the epoxy coating (Ep) or with epoxy directly blended with FND (Ep-FND-B). Here, the coating surfaces were cleaned using ear-washing bulbs and water before the tests to remove the loosely attached nanoparticles.

Characterization

Raman spectroscopy. Raman spectroscopy measurement of FND was performed on a Raman microscope system (LabRAM ARAMIS) with an Nd:YAG laser (532 nm) and an actual output power of 148 mW. The spectroscopy was collected at 32 scans, and the resolution was 4 cm^{-1}.

Fourier transform infrared spectroscopy (FTIR). FTIR spectra were obtained using a VECTOR-22 IR spectrometer (Bruker) at a resolution of 4 cm^{-1} with 64 scans to examine the surface compositions of the materials.

Surface morphology studies. The surface and cross-sectional morphology of the samples were detected using scanning electron microscope (SEM) (Zeiss, Pro G3, Germany) at an accelerating voltage of 10 kV. Energy dispersive spectroscopy (EDS) spectra of the coatings were carefully examined with the SEM at an accelerating voltage of 20 kV. The observation of FND by SEM was also used with this method. The 3D topographies of the coatings were ascertained with a dual-mode 3D optical profiler (RTEC Up, RTEC Ltd., USA).

Contact angle test. The water contact angle (WCA) and oil contact angle (OCA) were recorded with a Theta Auto 113 (KSV, Biolin) using 5 μL of deionized water and 3 μL of n-hexadecane respectively. The roll-off angle was measured with an OCA50 Micro (Dataphysics) using 10 μL of water. Each sample was measured five times at different positions to obtain an average value at room temperature.

Anticorrosion test. The anticorrosion property of the coatings was determined by chloride ion permeability tests (Chi et al., 2020). Epoxy solution was coated on one face of columned concrete specimen with the same dosage and curing time in the aforementioned tests. After curing, the specimen was saturated with water under vacuum, and paraffin was applied to the curved surfaces of the discs in case water and ions leak from the specimen. The chloride permeability was measured by using NEL-PDR concrete permeability tester (Naier Instruments) according to ASTM C 1202. Each coating was measured with three specimens to obtain an average value.

Stability test. The chemical stability of the superhydrophobic coating was examined by measuring the CAs of different pH droplets. Solutions with different pH values were prepared using HCl and NaOH. The cold resistance of the superhydrophobic coating was examined by measuring the WCA after the samples were frozen in a freezer for different durations. A mortar specimen covered with the superhydrophobic coating was placed in the freezer (−15°C) and then removed every 6 h; the WCA was measured when the sample recovered to room temperature. The CAs of different everyday liquids were also measured to evaluate the resistance of the coating to contaminants.

Adhesion test. The adhesion of the adhesive to the substrates was characterized using the pull-off test according to ASTM D7234. The adhesive was applied on a mortar specimen, and a 20-mm-diameter

cylindrical aluminum studs were then glued on the coating. Subsequently, the specimen was cured at room temperature for 14 d. The pull-off strength was measured by using a PosiTest AT-A pull-off adhesion tester (DeFelsko, USA). The pull rate was set as 0.2 MPa/s. Five different points on each sample were tested to obtain an average value.

Tape-peeling test. Adhesive tape was pressed onto the surface of Ep-FND-S (40 × 40 mm) with 100 g of weight to ensure good contact between the tape and the surface; then, the tape was peeled off. The WCA was measured after every 10 iterations of peeling.

Abrasion resistance test. The abrasion resistance of the fabricated superhydrophobic coating was examined through sandpaper abrasion. A mortar specimen covered with the superhydrophobic coating was placed face down onto an 800-mesh sandpaper with a load of 200 g. Then, the mortar was moved 10 cm forward by hand, rotated by 180°, and moved another 10 cm forward. This process was defined as one cycle. The WCA was tested after every 10 abrasion cycles to evaluate the abrasion resistance of the superhydrophobic coating.

Anti-icing test. The anti-icing properties of the coatings were examined by measuring the adhesion strength of icicles. Each sample was placed in the freezer, in which the temperature was set as −15°C. A φ15 × 15 mm cylinder treated with the hydrophobic reagent was positioned on the surface of the sample, and 1 mL of deionized water was injected into the cylinder. After freezing for 4 h, any icicles that had formed were removed by a horizontal shear force that was recorded using a dynamometer. The horizontal shear force was defined as the ice adhesion strength. Each sample was measured five times at different positions to obtain an average value.

Self-cleaning test. A sample was placed on a piece of paper at a certain tilt angle. Yellow pigment serving as a contaminant was evenly spread to completely cover the surface of the sample. Then, water was dropped on the surface using a syringe to test the self-cleaning effect of the prepared superhydrophobic coating by removing the yellow pigment. For comparison, the self-cleaning abilities of the other samples were also tested. Photographs of the samples at different moments were obtained.